Physics of Plasmas

Time integrator agnostic charge conserving finite element PIC

Cite as: Phys. Plasmas **28**, 092111 (2021); https://doi.org/10.1063/5.0046842
Submitted: 10 February 2021 • Accepted: 18 August 2021 • Published Online: 17 September 2021

Scott O'Connor, Zane D. Crawford, O. H. Ramachandran, et al.

View Online Export Citation CrossMark

ARTICLES YOU MAY BE INTERESTED IN

Dispersion relation for gauge-free electromagnetic drift kinetics
Physics of Plasmas **28**, 092504 (2021); https://doi.org/10.1063/5.0058118

Generalized Boozer coordinates: A natural coordinate system for quasisymmetry
Physics of Plasmas **28**, 092510 (2021); https://doi.org/10.1063/5.0060115

Hamiltonian fluid reduction of the 1.5D Vlasov–Maxwell equations
Physics of Plasmas **28**, 092114 (2021); https://doi.org/10.1063/5.0056155

Physics of Plasmas
Papers from 62nd Annual Meeting of the
APS Division of Plasma Physics
Read now!

AIP Publishing

© 2021 Author(s).

Physics of Plasmas ARTICLE scitation.org/journal/php

Time integrator agnostic charge conserving finite element PIC

Cite as: Phys. Plasmas **28**, 092111 (2021); doi: 10.1063/5.0046842
Submitted: 10 February 2021 · Accepted: 18 August 2021 ·
Published Online: 17 September 2021

View Online Export Citation CrossMark

Scott O'Connor,[a),b)] Zane D. Crawford,[b)] O. H. Ramachandran,[b)] John Luginsland, and B. Shanker

AFFILIATIONS

Department of Electrical and Computer Engineering, Michigan State University, Engineering Building, 428 S Shaw Ln, East Lansing, Michigan 48824, USA

[a)]**Author to whom correspondence should be addressed:** oconn220@msu.edu
[b)]**Also at:** Department of Computational Science, Mathematics, and Engineering, Michigan State University, Engineering Building, 428 S Shaw Ln, East Lansing, MI 48824, USA.

ABSTRACT

Developing particle-in-cell (PIC) methods using finite element basis sets, and without auxiliary divergence cleaning methods, was a long-standing problem until recently. It was shown that if consistent spatial basis functions are used, one can indeed create a methodology that was charge conserving, *albeit* using a leapfrog time stepping method. While this is a significant advance, leapfrog schemes are *only* conditionally stable and time step sizes are closely tied to the underlying mesh. Ideally, to take full advantage of advances in finite element methods (FEMs), one needs a charge conserving PIC methodology that is *agnostic* to the time stepping method. This is the principal contribution of this paper. In what follows, we shall develop this methodology, prove that both charge and Gauss' laws are discretely satisfied at every time step, provide the necessary details to implement this methodology for both the wave equation FEM and Maxwell solver FEM, and finally demonstrate its efficacy on a suite of test problems. The method will be demonstrated by single particle evolution, non-neutral beams with space-charge, and adiabatic expansion of a neutral plasma, where the Debye length has been resolved, and real mass ratios are used.

Published under an exclusive license by AIP Publishing. https://doi.org/10.1063/5.0046842

I. INTRODUCTION

Simulation of space charge and plasmas is critical to a number of areas in science and engineering. These range from applications of pulsed power to particle accelerators to satellites and medicine.[1–3] The means to do so has largely relied on particle-in-cell (PIC) methods. PIC has been around since the 1950s and is a popular method of modeling plasma and space charge due to its simplicity and ease of use.[4] PIC enables a self-consistent solution to Maxwell's equation and equations of motion for charged species. Traditionally, PIC is based on finite difference time domain (FDTD) to evolve fields.[5] The use of regular cubical grids presents challenges, especially in modeling complex geometry. Modeling curved features requires small cell sizes, and this results in a stair-stepped approximation of the desired geometry as well as small time steps in keeping with the Courant–Friedrichs–Lewy condition. Using cut-cells has improved the geometry representation by allowing boundaries to cut across cells.[6] Complex and fine features, as well as multi-scale objects, require the use of a prohibitively expensive number of small cells for high fidelity simulations. As a result of these challenges, there has been persistent investigation into the use of more sophisticated field evolution techniques.[7–10] A natural choice is using a time domain finite-element method (TDFEM) due to (a) unconditionally stable time stepping methods, (b) ability to model complex geometries, and (c) well developed extensions to higher order (both in representation of fields and geometry).[11]

While TDFEM can be thought of as a panacea for modeling complex geometries, it is not so for crucial quantities that must be conserved. These include Gauss' law and charge conservation. Indeed, developing a numerical scheme that implicitly conserved charge was an unsolved problem until the developments published in Refs. 12 and 13. Prior to this development, one used divergence cleaning methods to remove spurious charge accumulation.[14] The key to realizing charge conservation relied on (a) following the *de-Rham* sequence to represent physical quantities on a mesh, (b) write the equations to be solved as a collection of first order ordinary differential equations, and (c) interpret time integrals of currents as path integrals.[15] A more recent paper summarizes conditions that should be satisfied by self-consistent charge conserving schemes[16] and illustrates these conditions for different PIC schemes. As alluded to before, the TDFEM-PIC[12,13] method relies on Maxwell solvers in that one solves Maxwell's first order equations, as opposed to the wave equation,

Published under an exclusive license by AIP Publishing

and exploits leapfrog time stepping. The structure of the solver is such that one avoids a time growing null space corresponding to DC modes. The path integral of the current is interpreted in the average sense and is a consequence of the low order integrator. Unfortunately, leapfrog time stepping is only conditionally stable. As a result, there is a limit on the time step sizes that one can take, and this closely tied to the underlying discretization. In classical TDFEM field solvers, this has been overcome using Newmark-beta time stepping, which is second order and *unconditionally* stable. Unfortunately, implicit time stepping poses a number of challenges to satisfaction of conservation laws that must be satisfied and is an open problem.[17] This paper provides the focuses on providing a framework for resolving this bottleneck and creating consistency between field solution and field sources from the particles.

Implicit time stepping field solvers permits taking significantly larger time steps and un-constrained by the mesh; unconditional stability is an added bonus. Unfortunately, as will be evident in the paper, applying these directly to TDFEM-PIC violates both Gauss' law and the equation of continuity. In addition, in solving the field equations, one needs to evolve the locations of particles over time via Newton's laws. A larger time step size implies that additional infrastructure needs to be in place to accurately compute all aspects of particle trajectory (including information necessary to map it back on the mesh). Resolution to these challenges associated implicit time stepping with a TDFEM framework will be the main contribution of this paper.

1. We will develop the method to ensure that both Gauss' law and equation of continuity is satisfied for implicit field solvers. The methods rely on insight provided in Ref. 16. There are subtle nuances between the work in Refs. 15, 18, and 19 and what is presented here; specifically, for implicit transient field solvers, we need to ensure that the right hand side is constructed such that it is compatible with the Newmark–Beta (or any other) time stepping method used for the field solution.
2. We will show that the proposed method is agnostic to time stepping schemes used for the field solution.
3. We will develop methods to evolve particle parameters (path, velocity along the path, and mapping path to the mesh).
4. Finally, we will present results validating these methods for *both* the Maxwell and wave equation TDFEM solvers.

Our hope is to present the technique with sufficient lucidity such that they can be retrofitted with existing codes.

The rest of this paper is organized as follows: In Sec. II, we present an overall rubric of implicit TDFEM solvers (both Maxwell and wave equation), and why direct application of implicit time stepping fails to conserve quantities. Next, in Sec. III, we present details on how these may be modified so as to conserve charge, satisfy Gauss' law, and be independent of time stepping approach. In addition, we present details of the method used to evolve particle parameters. In Sec. IV, we present a number of results that validate our claims. Finally, we conclude this paper in Sec. V outlining future directions of research.

II. PRELIMINARIES

Consider a domain Ω whose boundaries are denoted by $\partial\Omega$. It is assumed that the domain comprise charged species that exist in a background medium defined by ε_0 and μ_0, the permittivity and permeability of free space, and the speed of light denoted using $c = 1/\sqrt{\mu_0\varepsilon_0}$; for simplicity of the exposition, we consider only one species. It is also assumed that there exists an electromagnetic field, both impressed and arising from motion of the charged species. Both the fields and the charged species evolve in time. The distribution of charge can be represented by a phase space distribution function (PSDF) $f(t,\mathbf{r},\mathbf{v})$ that satisfies the Vlasov equation

$$\partial_t f(t,\mathbf{r},\mathbf{v}) + \mathbf{v}\cdot\nabla f(t,\mathbf{r},\mathbf{v}) + \frac{q}{m}[\mathbf{E}(t,\mathbf{r}) + \mathbf{v}\times\mathbf{B}(t,\mathbf{r})]\cdot\nabla_v f(t,\mathbf{r},\mathbf{v}) = 0. \tag{1}$$

While we do not solve this equation directly, our approach is conventional in that we make a particle approximation for the PSDF in Eq. (1).

A. Overview of method

Using this PSDF, we follow the conventional definition of the charge and current density defined as $\rho(t,\mathbf{r}) = q\int_\Omega f(t,\mathbf{r},\mathbf{v})d\mathbf{v}$ and $\mathbf{J}(t,\mathbf{r}) = q\int_\Omega \mathbf{v}(t) f(t,\mathbf{r},\mathbf{v})d\mathbf{v}$ as moments of the PSDF. The fields, $\mathbf{E}(t,\mathbf{r})$ and $\mathbf{B}(t,\mathbf{r})$, in the Vlasov equation are solutions to Maxwell's curl equations with the sources (charge and currents) defined earlier

$$-\frac{\partial\mathbf{B}(t,\mathbf{r})}{\partial t} = \nabla\times\mathbf{E}(t,\mathbf{r}), \tag{2a}$$

$$\frac{\partial\mathbf{D}(t,\mathbf{r})}{\partial t} = \nabla\times\mathbf{H}(t,\mathbf{r}) - \mathbf{J}(t,\mathbf{r}), \tag{2b}$$

and boundary conditions. These can be either Dirichlet or impedance boundary conditions on $\partial\Omega_D$ or $\partial\Omega_I$, to bound the domain,

$$\hat{n}\times\mathbf{E}(\mathbf{r},t) = \mathbf{\Psi}_D(\mathbf{r},t) \text{ on } \partial\Omega_D, \tag{3a}$$

$$\hat{n}\times\frac{\mathbf{B}(\mathbf{r},t)}{\mu} - Y\hat{n}\times\hat{n}\times\mathbf{E}(\mathbf{r},t) = \mathbf{\Psi}_I(\mathbf{r},t) \text{ on } \partial\Omega_I, \tag{3b}$$

where Y is the admittance of free space. Instead of using Eq. (2), the wave equation

$$\nabla\times\left(\frac{1}{\mu_r}\nabla\times\mathbf{E}\right) + \frac{1}{c_0^2}\epsilon_r\frac{\partial^2\mathbf{E}}{\partial t^2} = -\mu_0\frac{\partial\mathbf{J}}{\partial t}, \tag{4}$$

can be used instead. The magnetic field can be obtained from Eq. (2a), and the impedance boundary condition is defined using a time derivative on Eq. (3b) and using Eq. (2a). The fields should also satisfy Gauss' laws

$$\nabla\cdot\mathbf{D}(t,\mathbf{r}) = \rho(t,\mathbf{r}), \tag{5}$$

$$\nabla\cdot\mathbf{B}(t,\mathbf{r}) = 0, \tag{6}$$

though they are not explicitly solved.

As alluded to earlier, we use the moments of the PSDF to find the fields and then evolve the system using Newton's equations and Lorentz force, $\mathbf{F}(t,\mathbf{r}) = q(t,\mathbf{r})(\mathbf{E}(t,\mathbf{r}) + \mathbf{v}(t,\mathbf{r})\times\mathbf{B}(t,\mathbf{r}))$, for the duration of the simulation. Thus far, our description has been in continuous world. To perform an actual simulation, we would need to represent all the quantities involved in terms of functions defined on a discretization of space and time. This is typically referred to as a particle in cell (PIC) approach and is the subject of our next discussion.

Our starting point is the representation of both Ω and $\partial\Omega$ in terms of a finite set of tetrahedra or a mesh that contains N_s nodes, N_e

Published under an exclusive license by AIP Publishing

edges, and N_f faces. On these tetrahedra, we define basis functions that follow the de-Rham sequence, enabling us to represent fields, fluxes, and sources. However, before proceeding too far ahead, note that we are going to follow the usual PIC cycle: (a) map charges and currents on the mesh, (b) solve for electric and magnetic fields on the mesh, (c) move particles due to Lorentz force and find the current due to this motion, and (d) find the fields due the updated sources. The cycle then continues.

The starting point of the simulation is to define the charge and currents due to PSDF. With no loss of generality, we follow the usual procedure such that $\rho(t,\mathbf{r}) = q_\alpha \sum_{p=1}^{N_p} \delta(\mathbf{r}-\mathbf{r}_p)$ and $\mathbf{J}(t,\mathbf{r}) = q_\alpha \sum_{p=1}^{N_p} \mathbf{v}_p(t)\delta(\mathbf{r}-\mathbf{r}_p)$. This implies that PSDF is sampled with N_p shape functions, each being a delta function. Generalization to other shape functions is possible[16] and is agnostic to the crux of this paper.

The electric and magnetic fields are represented using Whitney basis functions.[8,11,12] Specifically, the electric fields using Whitney edge basis functions $\mathbf{E}(t,\mathbf{r}) = \sum_{i=1}^{N_e} e_i(t)\mathbf{W}_i^{(1)}(\mathbf{r})$. The magnetic flux density is represented using the Whitney face basis function $\mathbf{B}(t,\mathbf{r}) = \sum_{i=1}^{N_f} b_i(t)\mathbf{W}_i^{(2)}(\mathbf{r})$. Here, N_e is the number of edges and N_f is the number of faces in the mesh. Two different approaches can be used to solve Maxwell's equations: (a) either solve them in the coupled form or (b) solve the wave equation for the electric field and then obtain the magnetic field. To set the stage for both these solvers, we introduce the following Hodge matrix operators:

$$[\star_\epsilon]_{i,j} = \langle \mathbf{W}_i^{(1)}(\mathbf{r}), \varepsilon \cdot \mathbf{W}_j^{(1)}(\mathbf{r})\rangle, \tag{7}$$

$$[\star_{\mu^{-1}}]_{i,j} = \langle \mathbf{W}_i^{(2)}(\mathbf{r}), \mu^{-1} \cdot \mathbf{W}_j^{(2)}(\mathbf{r})\rangle, \tag{8}$$

the surface impedance matrix

$$[\star_I]_{i,j} = \langle \hat{n}_i \times \mathbf{W}_i^{(1)}(\mathbf{r}), \mu^{-1} \cdot \hat{n}_j \times \mathbf{W}_j^{(1)}(\mathbf{r})\rangle, \tag{9}$$

and discrete curl operator

$$[\nabla \times]_{i,j} = \langle \hat{\mathbf{n}}_i, \nabla \times \mathbf{W}_j^{(1)}(\mathbf{r})\rangle, \tag{10}$$

where $\hat{n}_i$ is the surface normal on boundary of the domain of support for $\mathbf{W}_i^{(1)}(\mathbf{r})$ and $\langle\cdot,\cdot\rangle$ is an inner product defined as $\langle \mathbf{g}(\mathbf{r}), \mathbf{f}(\mathbf{r})\rangle = \int_v \mathbf{g}(\mathbf{r}) \cdot \mathbf{f}(\mathbf{r}) d\mathbf{r}$. These matrices are used to build the semidiscrete Maxwell system

$$\overline{\overline{C}}_M \begin{bmatrix} \partial_t \overline{B}(t) \\ \partial_t \overline{E}(t) \end{bmatrix} + \overline{\overline{K}}_M \begin{bmatrix} \overline{B}(t) \\ \overline{E}(t) \end{bmatrix} = \overline{\overline{F}}_M, \tag{11}$$

where

$$\bar{\bar{C}}_M = \begin{bmatrix} [I] & 0 \\ 0 & [\star_{\epsilon_0}] \end{bmatrix}, \tag{12}$$

$$\bar{\bar{K}}_M = \begin{bmatrix} 0 & [\nabla\times] \\ [\nabla\times]^T [\star_{\mu^{-1}}] & 0 \end{bmatrix}, \tag{13}$$

and $\overline{\overline{F}}_M = [0 - \bar{J}^T(t)]$. The degree of freedom vectors $\bar{E}(t) = [e_1(t), e_2(t), \ldots, e_{N_e}(t)]$, $\bar{B}(t) = [b_1(t), b_2(t), \ldots, b_{N_f}(t)]$, and $\bar{J}(t) = [j_1(t), j_2(t), \ldots j_{N_e}(t)]$ with $j_i(t) = \langle \mathbf{W}_i^{(1)}(\mathbf{r}), \mathbf{J}(t,\mathbf{r})\rangle$. The choice of measurement of the current density arises from not only the natural construction of the finite element system but the important interplay with the measurement of the charge density. The nodal basis set $W_i^{(0)}(\mathbf{r})$ measures $\rho(t,\mathbf{r})$ such that $\bar{\rho}(t) = [\rho_1(t), \rho_2(t), \ldots, \rho_{N_s}(t)]$, where $\rho_i(t) = \langle W_i^{(0)}(\mathbf{r}), \rho(t,\mathbf{r})\rangle$. The discrete system in (11) is the finite element representation of Maxwell equations and will subsequently be called the Mixed Finite Element Method (MFEM). For the wave equation, the system becomes

$$\underbrace{[\star_{\epsilon_0}]}_{\overline{\overline{M}}_W} \partial_t^2 \overline{E}(t) + \underbrace{c[\star_I]}_{\overline{\overline{C}}_W} \partial_t \overline{E}(t) + \underbrace{c^2[\star_S]}_{\overline{\overline{K}}_W} \overline{E} = -\partial_t \overline{J}(t), \tag{14}$$

where $[\star_S] = [\nabla\times]^T [\star_{\mu^{-1}}] [\nabla\times]$.

B. Unconditionally stable time marching

The mixed finite element system in Eq. (2) is discretized in time using Newmark–Beta, an unconditionally stable time stepping method. This method has been extensively used in wave equation[11] and examined for the mixed finite element method in Ref. 20, allowing for much larger time step sizes than the traditional leapfrog method. In this method, $\bar{E}(t)$ and $\bar{B}(t)$ are represented in time in terms of second order Lagrange polynomials such that for $t \in [t_{n-1}, t_{n+1}]$,

$$\begin{pmatrix} \bar{B}(t) \\ \bar{E}(t) \end{pmatrix} = \sum_{k=0}^{2} N_{n,k}(t) \begin{pmatrix} \bar{B}(t_{n+k-1}) \\ \bar{E}(t_{n+k-1}) \end{pmatrix}, \tag{15a}$$

$$L_{n,k}(t) = \prod_{\substack{j=0 \\ j\neq k}}^{2} \frac{t - t_{n+1-j}}{t_{n+1-k} - t_{n+1-j}}, \tag{15b}$$

$$N_{n,k}(t) = \begin{cases} L_{n,k}(t) & t \in [t_{n-1}, t_{n+1}], \\ 0 & \text{otherwise.} \end{cases} \tag{15c}$$

The governing set of differential equations in Eq. (11) is then tested by

$$T(t) = \begin{cases} \dfrac{t_n - t}{\Delta t} & t \in [t_{n-1}, t_n], \\ \dfrac{t - t_n}{\Delta t} & t \in [t_n, t_{n+1}], \\ 0 & \text{otherwise.} \end{cases} \tag{16}$$

This choice of basis and testing functions creates a non-dissipative, unconditionally stable time marching scheme, which can be written as a recurrence formula provided in Ref. 21, corresponding to parameters $\gamma = 0.5$ and $\beta = 0.25$. When applied to Eq. (11), this becomes

$$\begin{aligned} &\left(0.5\overline{\overline{C}}_M + 0.25\Delta_t \overline{\overline{K}}_M\right)\overline{X}^{n+1} - 0.5\Delta_t \overline{\overline{K}}_M \overline{X}^n \\ &+ \left(0.5\overline{\overline{C}}_M + .025\Delta_t \overline{\overline{K}}_M\right)\overline{X}^{n-1} + 0.25\Delta_t \overline{F}_M^{n+1} \\ &+ 0.5\Delta_t \overline{F}_M^n + 0.25\Delta_t \overline{F}_M^{n-1} = 0, \end{aligned} \tag{17}$$

where $\bar{X}^m = [\bar{B}^T(t_m), \bar{E}^T(t_m)]$ and $\bar{F}_M^m = [0, -\bar{J}^T(t_m)]$ for $m \in [n-1, n+1]$ and $t_m = m\Delta_t$. Likewise, Eq. (14) becomes

$$\begin{aligned} &\left(\overline{\overline{M}}_W + 0.5\Delta_t \overline{\overline{C}}_W + 0.25\Delta_t^2 \overline{\overline{K}}_W\right)\overline{E}^{n+1} + \left(-2\overline{\overline{M}}_W - 0.5\Delta_t^2 \overline{\overline{K}}_W\right)\overline{E}^n \\ &\times \left(\overline{\overline{M}}_W + 0.5\Delta_t \overline{\overline{C}}_W + .025\Delta_t^2 \overline{\overline{K}}_W\right)\overline{E}^{n-1} \\ &+ 0.25\Delta_t^2 \overline{F}_W^{n+1} + 0.5\Delta_t^2 \overline{F}_W^n + 0.25\Delta_t^2 \overline{F}_W^{n-1} = 0. \end{aligned} \tag{18}$$

Published under an exclusive license by AIP Publishing

Both Eqs. (17) and (18) are outcomes of discretization of Maxwell's equations (or the corresponding wave equation) with either the current (or its derivative) on the right hand side. As written in the discrete form, it will not preserve the necessary link between Ampère's and Gauss' law necessary for charge conservation. This is immediately apparent after applying a discrete divergence operator to semidiscrete Ampère's law. Applying the discrete divergence operator on the Ampère's law portion of Eq. (17), and using the identity that $[\mathbf{\nabla}\cdot][\mathbf{\nabla}\times]^T = 0$, yields

$$0.5[\mathbf{\nabla}\cdot][\star_{\epsilon_0}]\bar{E}^{n+1} - 0.5[\mathbf{\nabla}\cdot][\star_{\epsilon_0}]\bar{E}^{n-1} = -0.25\Delta_t[\mathbf{\nabla}\cdot]\bar{J}^{n+1} - 0.5\Delta_t[\mathbf{\nabla}\cdot]\bar{J}^{n} - 0.25\Delta_t[\mathbf{\nabla}\cdot]\bar{J}^{n-1}. \quad (19)$$

When the same divergence operator is applied to discrete wave Eq. (19), one gets

$$[\mathbf{\nabla}\cdot][\star_{\epsilon_0}]\bar{E}^{n+1} - 2[\mathbf{\nabla}\cdot][\star_{\epsilon_0}]\bar{E}^{n} + [\mathbf{\nabla}\cdot][\star_{\epsilon_0}]\bar{E}^{n-1} -0.25\Delta_t[\mathbf{\nabla}\cdot]\bar{J}^{n+1} - 0.5\Delta_t[\mathbf{\nabla}\cdot]\bar{J}^{n} - 0.25\Delta_t[\mathbf{\nabla}\cdot]\bar{J}^{n-1}. \quad (20)$$

Note, Gauss' law is satisfied provided $\bar{\rho}^n = [\mathbf{\nabla}\cdot][\star_{\epsilon_0}]\bar{E}^n$ for any time step n. It is evident that both Eqs. (19) and (20) are incompatible with Gauss' laws. Instead, a different treatment of the right hand side, the particle current density, is needed in order to create a charge conserving scheme.

III. MODIFIED TDFEM-PIC

A. Integrator agnostic charge conserving scheme

It is apparent that, as written, charge conservation fails for both Maxwell solver and the wave equation. The reasons are twofold: (a) the order of time derivatives on the current (on the right hand side) and those on the electric field are off by one; (b) this requires the discrete time integrator to remember initial conditions. The latter holds the key to solving the puzzle. Newmark time stepping schemes are, in effect, stable time integrators. The crux of our approach is to correctly evaluate the time integral of the current. As elucidated in Ref. 16, the time integral of the current is obtainable and indeed a part of the PIC scheme. Specifically, starting with the definition of the PSDF,

$$\rho(t,\mathbf{r}) = -\mathbf{\nabla}\cdot\int_0^t \mathbf{J}(\tau,\mathbf{r})d\tau. \quad (21)$$

As shown in Ref. 16, this equation can be rewritten as

$$\rho(t,\mathbf{r}) = -\mathbf{\nabla}\cdot\int_{\mathbf{r}(0)}^{\mathbf{r}(t)} \mathbf{J}(\tilde{\mathbf{r}})d\tilde{\mathbf{r}}. \quad (22)$$

Following the details in Ref. 16, it is immediately apparent that for any particle p, the path integral at t_n is

$$\int_0^{t_n} d\tau \mathbf{v}_p(\tau)\delta\big(\mathbf{r}-\mathbf{r}_p(\tau)\big) = \int_{\mathbf{r}_p(0)}^{\mathbf{r}_p(t_n)} d\tilde{\mathbf{r}}\delta(\mathbf{r}-\tilde{\mathbf{r}}). \quad (23)$$

Note, for each charge, its trajectory is determined by the solution to Newton's equations. The integration along a particle path can be computed to a high degree of accuracy. To develop a charge conserving methodology, we define

$$\mathbf{G}(t,\mathbf{r}) = \int_0^t \mathbf{J}(\tau,\mathbf{r})d\tau. \quad (24)$$

As is evident from Eq. (23), this integral can be converted into a path integral. The evaluation of this path integral is effected numerically as described in Sec. III B. We should note that the order of the numerical scheme is such that it is greater than the order of time derivatives on $\mathbf{G}(t,\mathbf{r})$. It follows that instead of using $\bar{J}$ in Eq. (11) [and, therefore, in Eq. (20)], one can instead use $\partial_t\bar{G}(t)$, where $\bar{G}(t) = [g_1(t), g_2(t), \ldots, g_{N_e}(t)]$ with $g_i(t) = \langle \mathbf{W}_i^{(1)}(\mathbf{r}), \mathbf{G}(t,\mathbf{r})\rangle$. Discrete implementation with a Maxwell equation solver results in the divergence of Ampère's law to be

$$0.5[\mathbf{\nabla}\cdot][\star_{\epsilon_0}]\bar{E}^{n+1} - 0.5[\mathbf{\nabla}\cdot][\star_{\epsilon_0}]\bar{E}^{n-1} = +.5[\mathbf{\nabla}\cdot]\bar{G}^{n+1} - 0.5[\mathbf{\nabla}\cdot]\bar{G}^{n-1}. \quad (25)$$

Examining (26) term by term reveals that both sides of the equation are identical given that $[\mathbf{\nabla}\cdot]\bar{G}^n = -\bar{\rho}^n$. In a similar manner, one can use $\partial_t^2\bar{G}$ instead of $\partial_t\bar{J}$ in Eq. (15) to yield

$$\bar{\rho}^{n+1} - 2\bar{\rho}^n + \bar{\rho}^{n-1} = -[\mathbf{\nabla}\cdot]\bar{G}^{n+1} - 2[\mathbf{\nabla}\cdot]\bar{G}^{n} + [\mathbf{\nabla}\cdot]\bar{G}^{n-1}. \quad (26)$$

Here, we have taken the liberty of substituting, $\bar{\rho}^n = [\nabla\cdot][\star_{\epsilon_0}]\bar{E}^n$. At this point, we note that the proposed approach is agnostic to the time stepping scheme (or integrator) used to solve Maxwell's equations; both the equation of continuity and Gauss' laws are satisfied by design.

There is a subtle but key difference between the work in this paper and the others[15,18,19] in the origin of $\bar{G}^n$. In general, these arise from posing the Maxwell's equations in terms of set of first order equations and then using an appropriate temporal integrator. It can be shown via Eq. (23) that the time integral of the current transforms to a path integral. However, it is well known that this approach leads to conditionally stable field solution, with time step sizes determined by the smallest eigenvalue of the FEM system. To ensure compatibility (so as to be charge conserving) with unconditionally stable field solvers (be it Maxwell or the wave equation), we have to take this notion a few steps further. Knowing that the solution to the system is in effect an integrator, we introduce an auxiliary variable $\bar{G}^n$ that is evaluated via a path integral and then use as many time derivatives as necessary so as to be compatible with field solvers. This subtle but not so trivial insight creates a method that is applicable for both Maxwell and wave-equation FEM solvers. Note, if we use a leapfrog time stepping method, the equation resulting from Villasenor–Buneman (and its others)[15,18,19,22] and this paper will result in the same right hand side.

A word of caution is in order before we proceed. While the method developed is exact, it should be noted that to obtain $\bar{E}^{n+1}$, one needs to solve either (17) or (18) with the appropriate substitutions for $\bar{G}^{n+1}$ instead of $\bar{J}^{n+1}$. Obviously, the solution to these sets of equations is subject to errors that arise due to vagaries of a linear algebraic solution (tolerances, excitation of null-spaces, etc.). Consequently, as will be seen in Sec. IV, our errors are small but not identically zero. Next, we discuss a higher order particle pusher to solve the equations of motion consistently.

B. Particle pusher

Using an implicit time stepping scheme has advantages as well as challenges. The principal advantage is an unconditionally stable time step size independent scheme as opposed to a conditionally stable

Published under an exclusive license by AIP Publishing

scheme like leapfrog whose stability depends on the time step size. The downside of using large time steps is that one must capture the nuances of both the path and velocity of the particle. Thus, solving the equations of motion using a Boris push[23] with its linear representation of the particle position and velocity can introduce large errors into the system. Our goal is to develop a higher order scheme.

As is well known, the particle positions and velocities are updated by solving Newton's equations via the Lorentz force, giving us the following set of coupled first order ODEs for each particle:

$$\partial_t \mathbf{v}_p(t,\mathbf{r}_p) = \mathbf{a}_p(t,\mathbf{r}_p) = \frac{q_\alpha}{m_\alpha}\left(\mathbf{E}(t,\mathbf{r}_p) + \mathbf{v}_p(t,\mathbf{r}_p)\times\mathbf{B}(t,\mathbf{r}_p)\right), \quad (27)$$

$$\partial_t \mathbf{r}_p(t,\mathbf{r}_p) = \mathbf{v}_p(t,\mathbf{r}_p). \quad (28)$$

These form a pair of first order ODEs in time, and there are a number of methods that can be applied. Our choice is to use a higher order Adams–Bashforth scheme. An exemplar recursion relation for $\mathbf{v}$ and $\mathbf{r}$ for a fourth order Adams–Bashforth method is as follows:

$$\mathbf{v}_p^{n+1} = \mathbf{v}_p^n + \frac{\Delta_t}{24}\left(55\mathbf{a}_p^n - 59\mathbf{a}_p^{n-1} + 37\mathbf{a}_p^{n-2} - 9\mathbf{a}_p^{n-3}\right), \quad (29)$$

$$\mathbf{r}_p^{n+1} = \mathbf{r}_p^n + \frac{\Delta_t}{24}\left(55\mathbf{v}_p^n - 59\mathbf{v}_p^{n-1} + 37\mathbf{v}_p^{n-2} - 9\mathbf{v}_p^{n-3}\right), \quad (30)$$

where Δ_t is the time step size. Given that the Newmark scheme is second order, we choose the Adams-Bashforth scheme to be at least two orders higher so as to accommodate a second time derivative in on $\bar{G}^n$. The path used for interpolating the position is a fourth order Lagrange polynomial $k = 4 + 1$, which is defined as

$$\mathbf{r}_p(t) = \sum_{j=0}^{k} \mathbf{r}_p^{n-j}\ell_j(t), \quad (31a)$$

$$\ell(t) = \prod_{\substack{0\le m\le k\\ m\neq j}} \frac{t - t_{n+1-m}}{t_{n+1-j} - t_{n+1-m}}, \quad (31b)$$

where $\mathbf{r}_p(t)$ is the position at time t and $\mathbf{r}_p^n$ is the location of particle p at the $t = n\Delta_t$.

C. Particle path and current mapping

The final step is mapping the path to the underlying tessellation. In order to do so, we note that the integrator used to solve the equation of motion implicitly assumes a Lagrange polynomial interpolant. As a result, the order of the method used maps to order of the interpolant. This information needs to be used to find out where the particle enters and leaves the cell.

Once the particle locations at each time step are known from the particle push, the path through the unstructured mesh needs to be found. This includes finding the locations of where a particle enters a cell and where it leaves and is detailed in Algorithm 1. Since we are using a higher order representation of a particle path, finding these entry and exit points of the cell with the tetrahedron becomes a non-linear problem and is detail in Algorithm 2. Assume that we are given the normal to surface $\hat{\mathbf{n}}$, and vertices of the triangle $\mathbf{r}_{v,1}$, $\mathbf{r}_{v,2}$, $\mathbf{r}_{v,3}$. The intersection between the trajectory $\mathbf{r}_p(t)$ and the plane can be obtained by solving

$$\hat{\mathbf{n}}\cdot\left[\left(\mathbf{r}_p(t) - \mathbf{r}_{v,1}\right)\times\left(\mathbf{r}_{v,2} - \mathbf{r}_{v,1}\right)\right] = 0. \quad (32)$$

ALGORITHM 1. Particle path finding algorithm.

```
Push particle finding r_{p,f}
if r_{p,f} is in same cell as r_{p,s} then
    if All quadrature points between are in same cell then
        Integrate using a quadrature rule along path.
        Return and go onto next particle
    end if
end if
Find exit point r_{p,i} of path in cell
Integrate from r_{p,s} to r_{p,i}
while Path not complete do
    Find next cell that path travels through
    if r_f is in same cell as r_{p,i} then
        if All quadrature points are in same cell then
            Integrate using a quadrature rule along path.
            Path is complete
            Return and go onto next particle.
        else
            Find exit point of path in cell.
            Integrate from r_{p,is} to r_{p,if}.
        end if
    end if
end while
```

ALGORITHM 2. Non-linear bi-section method.

```
t_s = 0, t_f = 1, t_h = 0.5
if Any quadrature points are outside of the cell. then
    t_f = t_q
end if
while |t_s − t_f| < tol do
    if t_h is in same cell as t_s then
        t_s = t_h
    else
        t_f = t_h
    end if
    t_h = 0.5(t_s + t_f)
end while
```

Note the path $\mathbf{r}_p(t)$ can be parameterized using Eq. (31). Using this parameterization, one can use a non-linear iteration (such as Newton–Raphson) to solve (32). For convenience, we take a simpler approach by implementing a bi-section method that moves along the path checking whether candidate points are inside or outside of the cell. For test cases presented in this paper, this method converges rather robustly. Every step takes around 47 steps to converge below a tolerance of 1×10^{-15} ($0.5^{47} = 7.1\times10^{-15}$). Once the method converges, we then compute the integral along each path segment in each cell using a set of quadrature points. It should be noted that since each path segment is represented by a polynomial, the integral along

Published under an exclusive license by AIP Publishing

each path can be computed exactly using a high enough quadrature rule. To illustrate this, consider Fig. 1 containing an example particle starting position $\mathbf{r}_{p,s}$, and finishing position $\mathbf{r}_{p,f}$ with the intersection point being $\mathbf{r}_{p,i}$. The quadrature points would lie along the path between the $\mathbf{r}_{p,s}$ and $\mathbf{r}_{p,i}$ and then another set of quadrature points between $\mathbf{r}_{p,i}$ and $\mathbf{r}_{p,f}$.

Before we discuss results obtained using the above approach, a few points are in order to evaluate $\bar{G}^n$, (a) the integral over the path be evaluated using quadrature rules to very high precision as the order of the path is known; (b) when the path passes through multiple cells, the integration is broken up into pieces over each cell; (c) one can save on computational cost of by updating the integral.

D. Computational complexity

Next, we briefly discuss the asymptotic computational cost of the above algorithm. Assume for discussion purposes that there are N_p particles, N_s spatial degrees of freedom, and N_t time steps. Further, assume that given a right hand side, solution takes N_{it} iterations to reach a given threshold. It follows that for each time step, the solution to Maxwell's equations takes $\mathcal{O}(N_s N_{it})$ time, whereas the creation of the right hand side via the solution to Newton's takes $\mathcal{O}(N_p)$ as the number searches to find associated tetrahedra is $\mathcal{O}(1)$. Typically, the cost of the Maxwell solve dwarfs the cost of finding the path. Note, unfortunately, the cost of the Maxwell solve cannot be as good as FDTD, but FEM does have advantages alluded to earlier and it may be possible to leverage domain decomposition approaches to achieve better run time costs. In general, while the computational cost require to find the non-linear path presented in Sec. III C might be higher than a linear path, the fewer time steps required for the field solver out weights the cost of the particle mapper.

IV. RESULTS

In this section, we present a number of results demonstrating the efficacy of the proposed scheme with respect to conservation laws as well as accuracy of key steps that are integral to the process.

A. Higher order particle motion

One of the key advantages in using implicit time stepping is the possibility of using much larger time step sizes. Unfortunately, this also implies that one needs higher order methods to capture both the path and velocity. In this section, we demonstrate convergence of our algorithm for particle motion using various orders of an Adams–Bashforth integrator and compare these to standard non-relativistic Boris push. It should be noted that the Adams–Bashforth integrator, for the purposes of this paper, is run within its stable limits.

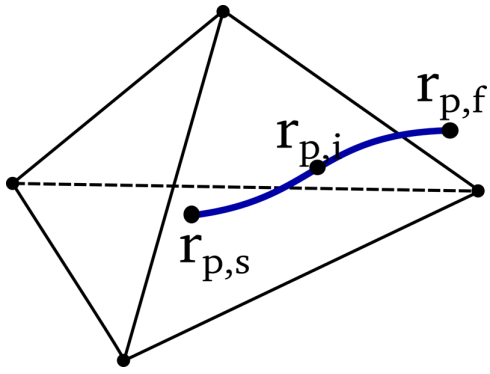

FIG. 1. Particle path for a single particles with start and location and intersection point.

TABLE I. Cyclotron motion.

Parameter	Value
$\mathbf{B}$	$6.822\,756 \times 10^{-5}\hat{z}$ T
Q	$-1.602\,176\,46 \times 10^{-19}$ C
m	$9.109\,383\,70 \times 10^{-31}$ kg
$\mathbf{v}_0$	$3 \times 10^{6}\hat{y}$ m/s
$\mathbf{r}_0$	$[0.75, 0.5, 0.0]$ m

To do so, we set up a classic cyclotron[24] motion test where a single particle was given an initial velocity in a constant magnetic field resulting in circular motion. The parameters are shown in Table I with a particle's initial velocity $\mathbf{v}_0$ with a background magnetic fields $\mathbf{B}$ with a given mass m and charge q. The particle will move in a circle due to the Lorentz force. The relative error in both position and velocity for various time step sizes with multiple order of Adams–Bashforth and Boris is shown in Figs. 2 and 3, respectively. The average error is calculated by taking the norm of the distance errors of each point $\mathbf{r}$ and dividing by the normal of the analytic positions $\mathbf{r}_a$ (see Ref. 24 for details),

$$error = \frac{||\mathbf{r} - \mathbf{r}_a||_2}{||\mathbf{r}_a||_2}. \tag{33}$$

The slopes for each of the Adams–Bashforth methods match its order. Boris, on the other hand, has a second order velocity update with a first order positional update. This test essentially validates the pusher as well as helps to correlate error (or approximately so) in particle motion with time step size. Note that Fig. 2 shows that a higher order

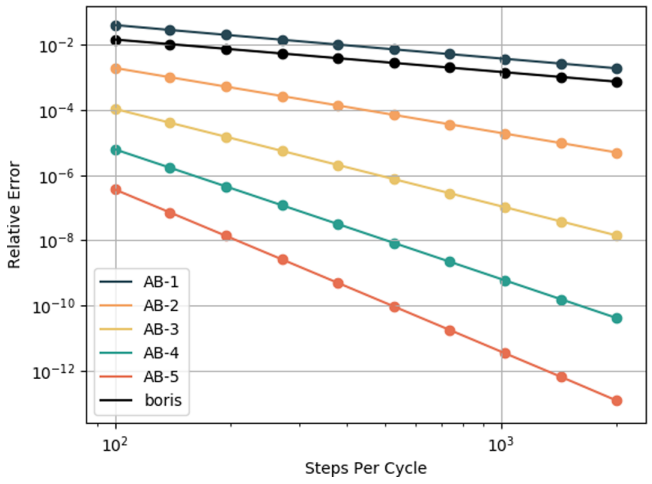

FIG. 2. Mean relative error in position for Adams–Bashforth orders 1–5 compared with the Boris push, shown in black.

Published under an exclusive license by AIP Publishing

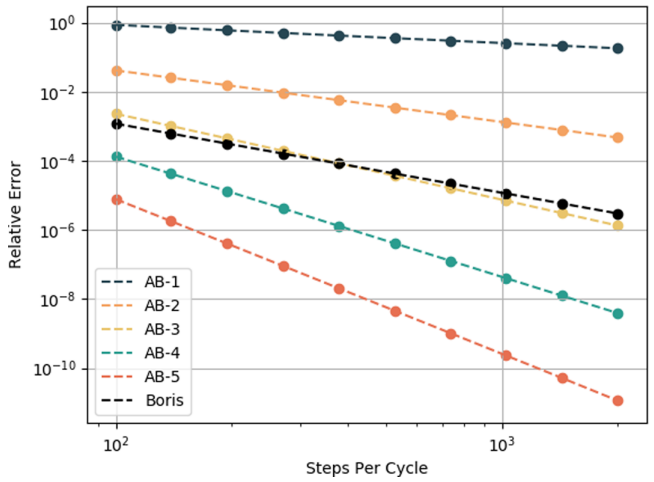

FIG. 3. Mean relative error in velocity for Adams–Bashforth orders 1–5 compared with the Boris push, shown in black.

time stepping method can take much larger time steps with smaller error than a lower order methods.

B. Expanding particle beam

Next, we consider an expanding beam test.[24] An expanding particle beam is injected into a cylindrical cavity with an initial velocity of magnitude v_0. As the beam travels down the tube, the electrons repel each other causing the beam to expand. This expansion rate can be compared with other codes to validate the solution. The detail of the mesh and beam parameters used is shown in Table II.

Both the wave equation and mixed finite element trajectories are compared in Fig. 4 and show good agreement with XOOPIC[5] (an extensively used and well validated quasi-2D FDTD code). We sample the electric field halfway down the tube 16 mm from the center of the tube. The radial field values are plotted over time shown in Fig. 5 for

TABLE II. Expanding particle beam parameters.

Parameter	Value
Cavity radius	20 mm
Cavity length	100 mm
Boundary conditions	Perfect electrical conductor
v_0	5×10^7 m/s
v_0/c	0.166 78
Beam radius r_b	8.00 mm
Number particles per time step	10
Species	Electrons
Turn on time	2 ns
Beam current	0.25 A
Macro-particle size	52 012.58
Min. edge length	1.529 mm
Max. edge length	6.872 mm
Δ_t	ns

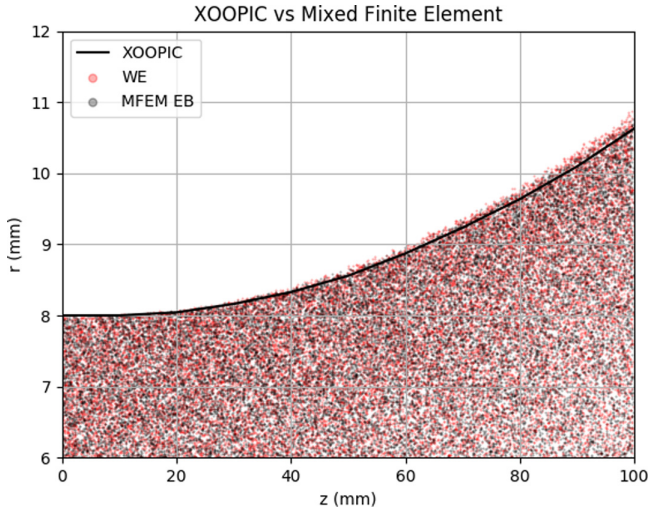

FIG. 4. Expanding particle beam macro-particles in the z vs r plan. Particle locations from both mixed finite element methods and wave equation versions are compared with XOOPIC beam profile.

simulations with different time steps. We compare four runs with time steps of $\alpha\Delta_t$ where α is scale factor and $\Delta_t = 0.333$ ps is the largest stable step size in a leapfrog time marching method for the given mesh. Note that 2 ns corresponds to 1 transit of the tube. It is evident from this figure that the proposed method provides stable results; indeed, as is evident from this figure, the data at $7.5\Delta_t$, $15\Delta_t$, and $30\Delta_t$ are almost identical to each other, where as the one at $1485\Delta_t$ is slightly different. This points to significant gains that can be made with Newmark time stepping (provided that the method is charge conserving).

This leads to the next argument. Shown in Fig. 6 are data from two different methods for the same setup run using with backward difference at Δ_t, MFEM with Newmark at $7\Delta_t$ and the wave equation (WE) at $7\Delta_t$. As evident, all three methods conserve charge to almost machine

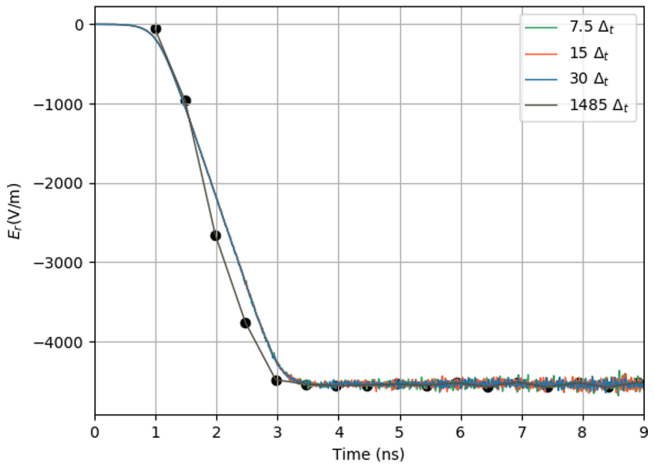

FIG. 5. Electric field values are the radial component halfway down the tube 16 mm from the center of the tube. Multiple simulation with different time steps is performed.

Published under an exclusive license by AIP Publishing

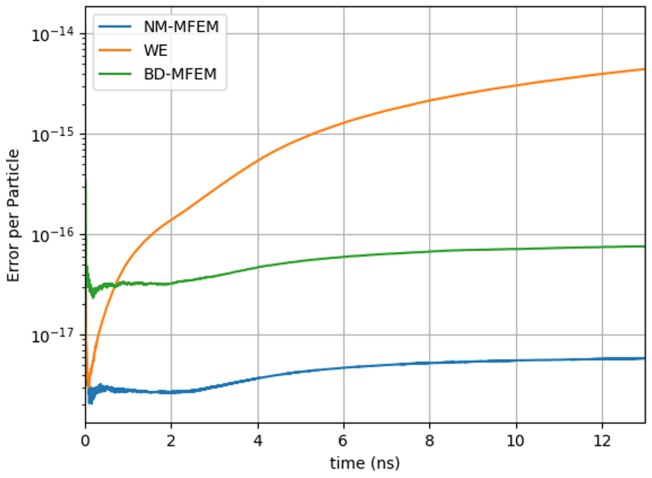

FIG. 6. Discrete Gauss's law error per particle for Newmark–Beta mixed finite element (NM-MFEM), Newmark–Beta wave equation (WE), backward difference mixed finite elements (BD-MFEM) using the charge conservation technique provided here.

precision. It should be noted that both MFEM and WE have a null space. In the case of the former, it is fields that behave like $\nabla\phi(\mathbf{r})$, and the latter, as $t\nabla\phi(\mathbf{r})$. However, as is evident from these results, our mapping on to these null spaces is small and behaves as expected.

To further illustrate the robustness of the method to time step sizes, in Fig. 7, we compare the satisfaction of Gauss' law for all four time steps used in Fig. 5. As is evident from here, charge is again conserved almost to machine precision (around 10^{-18} for all with slight difference evolution of trajectory).

C. Adiabatic expanding plasma

Finally, for a third validation case, we simulate an adiabatic expansion of a plasma ball with radial Gaussian distribution in the radial direction. This case has an analytic solutions[25] and allows for good comparison and validation. We change some of the parameters from the original numerical experiments[24] such that the Debye length can be fully resolved (Table III). This example is described in more detail in Ref. 24. We simulate both the examples MFEM and WE. For both the examples, we get excellent agreement in the expansion rate with both the wave equation, Fig. 8, and the mixed formulation, Fig. 9, when compared with analytic densities.

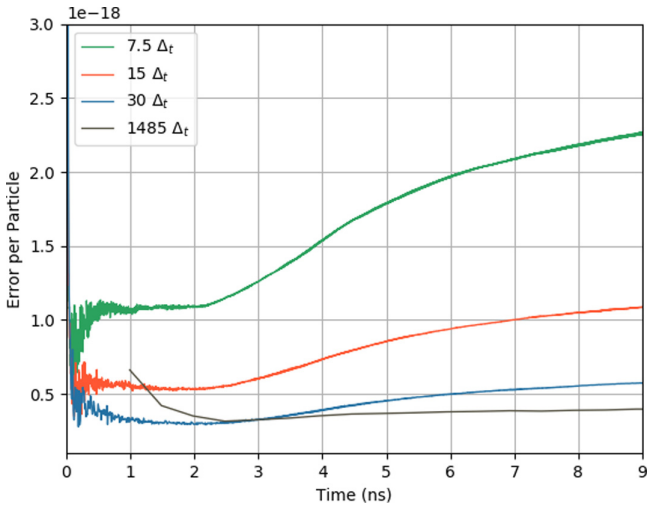

FIG. 7. Discrete Gauss's law error per particle various time steps using the mixed finite element methods using Newmark time stepping.

TABLE III. Adiabatic expanding plasmas.

Parameter	Value
Mesh radius	6 mm
Boundary conditions	First order ABC
T_{ion}	1 K
$T_{electron}$	100 K
Number particles	8000
Species	Electrons and Sr^{+}
Macro-particle size	52 012.58
Min. edge length	1.529 mm
Max. edge length	6.872 mm

V. SUMMARY

In this paper, we have presented a solution to a problem that has been long-standing–charge conserving FEM-PIC methods for implicit time stepping using a Newmark–Beta time stepping methods for both Maxwell and Wave equation based finite element solvers without the need to adopt divergence cleaning. In other words, rubrics have been developed such that conservation laws are implicitly obeyed. Indeed, the method presented is agnostic to any time stepping scheme used for field solution. We have demonstrated the efficacy of this approach for a set of test problems, using different time step sizes and different time stepping schemes, as well as both MFEM and WE solvers. The

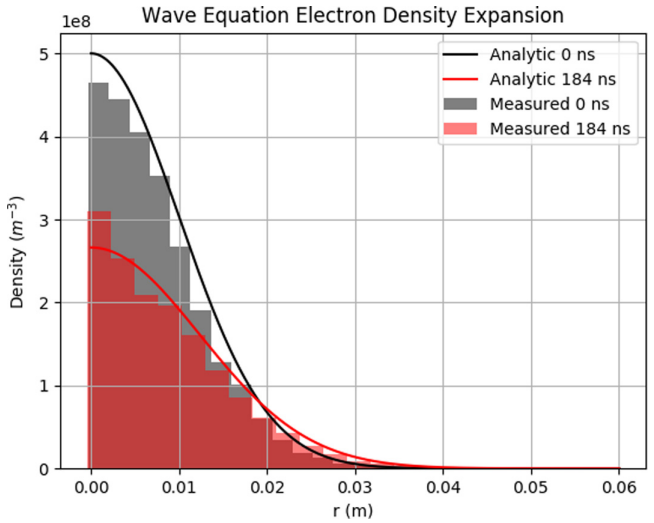

FIG. 8. Wave equation adiabatic expanding plasma.

Published under an exclusive license by AIP Publishing

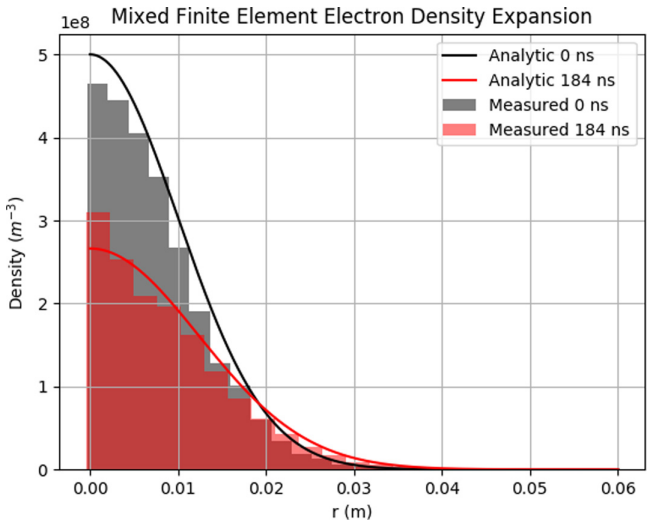

FIG. 9. Mixed finite element adiabatic expanding plasma.

results reliably attest our claims. The above approach opens multiple doors that will further the state of art of FEM-PIC; these include higher order schemes in both space and time, quasi-Helmholtz decomposition to get a better handle on null-spaces, and domain decomposition to effect rapid solution by parallelizing the scheme. Papers on these will be presented soon in other forums.

ACKNOWLEDGMENTS

This work was supported by SMART Scholarship program. The authors thank the MSU Foundation for support through the Strategic Partnership Grant during early portion of this work. This work was also supported by the Department of Energy Computational Science Graduate Fellowship under Grant No. DE-FG02-97ER25308 and financial support from NSF via No. CMMI-1725278. The authors would also like to thank the HPCC Facility, Michigan State University, East Lansing, MI, USA.

DATA AVAILABILITY

The data that support the findings of this study are available from the corresponding author upon reasonable request.

REFERENCES

[1]R. Marchand, "PTETRA, a tool to simulate low orbit satellite–plasma interaction," IEEE Trans. Plasma Sci. **40**, 217–229 (2011).
[2]R. Lemke, T. Genoni, and T. Spencer, "Three-dimensional particle-in-cell simulation study of a relativistic magnetron," Phys. Plasmas **6**, 603–613 (1999).
[3]E. Fourkal, B. Shahine, M. Ding, J. Li, T. Tajima, and C.-M. Ma, "Particle in cell simulation of laser-accelerated proton beams for radiation therapy," Med. Phys. **29**, 2788–2798 (2002).
[4]C. K. Birdsall and A. B. Langdon, *Plasma Physics via Computer Simulation* (CRC Press, 2004).
[5]J. P. Verboncoeur, "Particle simulation of plasmas: Review and advances," Plasma Phys. Controlled Fusion **47**, A231 (2005).
[6]C. Nieter, J. R. Cary, G. R. Werner, D. N. Smithe, and P. H. Stoltz, "Application of Dey–Mittra conformal boundary algorithm to 3D electromagnetic modeling," J. Comput. Phys. **228**, 7902–7916 (2009).
[7]J. Squire, H. Qin, and W. M. Tang, "Geometric integration of the Vlasov-Maxwell system with a variational particle-in-cell scheme," Phys. Plasmas **19**, 084501 (2012).
[8]P. Monk, *Finite Element Methods for Maxwell's Equations* (Oxford University Press, 2003).
[9]A. S. Glasser and H. Qin, "The geometric theory of charge conservation in particle-in-cell simulations," preprint arXiv:1910.12395 (2019).
[10]C. S. Meierbachtol, A. D. Greenwood, J. P. Verboncoeur, and B. Shanker, "Conformal electromagnetic particle in cell: A review," IEEE Trans. Plasma Sci. **43**, 3778–3793 (2015).
[11]J.-M. Jin, *The Finite Element Method in Electromagnetics* (John Wiley & Sons, 2015).
[12]M. C. Pinto, S. Jund, S. Salmon, and E. Sonnendrücker, "Charge-conserving FEM–PIC schemes on general grids," C. R. Mec. **342**, 570–582 (2014).
[13]H. Moon, F. L. Teixeira, and Y. A. Omelchenko, "Exact charge-conserving scatter–gather algorithm for particle-in-cell simulations on unstructured grids: A geometric perspective," Comput. Phys. Commun. **194**, 43–53 (2015).
[14]C.-D. Munz, P. Omnes, R. Schneider, E. Sonnendrücker, and U. Voss, "Divergence correction techniques for Maxwell solvers based on a hyperbolic model," J. Comput. Phys. **161**, 484–511 (2000).
[15]J. Villasenor and O. Buneman, "Rigorous charge conservation for local electromagnetic field solvers," Comput. Phys. Commun. **69**, 306–316 (1992).
[16]Z. D. Crawford, S. O'Connor, J. Luginsland, and B. Shanker, "Rubrics for charge conserving current mapping in finite element particle in cell methods," preprint arXiv:2101.12128 (2021).
[17]G. Chen, L. Chacón, and D. C. Barnes, "An energy-and charge-conserving, implicit, electrostatic particle-in-cell algorithm," J. Comput. Phys. **230**, 7018–7036 (2011).
[18]T. Z. Esirkepov, "Exact charge conservation scheme for particle-in-cell simulation with an arbitrary form-factor," Comput. Phys. Commun. **135**, 144–153 (2001).
[19]K. Kormann and E. Sonnendrücker, "Energy-conserving time propagation for a structure-preserving particle-in-cell Vlasov–Maxwell solver," J. Comput. Phys. **425**, 109890 (2021).
[20]Z. Crawford, J. Li, A. Christlieb, and B. Shanker, "Unconditionally stable time stepping method for mixed finite element Maxwell solvers," Prog. Electromagn. Res. **103**, 17–30 (2020).
[21]O. C. Zienkiewicz, "A new look at the Newmark, Houbolt and other time stepping formulas. a weighted residual approach," Earthquake Eng. Struct. Dyn. **5**, 413–418 (1977).
[22]J. Xiao and H. Qin, "Explicit structure-preserving geometric particle-in-cell algorithm in curvilinear orthogonal coordinate systems and its applications to whole-device 6d kinetic simulations of Tokamak physics," Plasma Sci. Technol. **23**, 055102 (2021).
[23]J. P. Boris, "Relativistic plasma simulation-optimization of a hybrid code," in *Proceedings of the Conference on the Numerical Simulation of Plasmas (4th)* (Naval Research Laboratory, Washington, DC, 1970), pp. 3–67.
[24]S. O'Connor, Z. Crawford, J. Verboncoeur, J. Lugisland, and B. Shanker, "A set of benchmark tests for validation of 3D particle in cell methods," preprint arXiv:2101.09299 (2021).
[25]V. Kovalev and V. Y. Bychenkov, "Analytic solutions to the Vlasov equations for expanding plasmas," Phys. Rev. Lett. **90**, 185004 (2003).

Published under an exclusive license by AIP Publishing